nature photonics

LETTERS

PUBLISHED ONLINE: 15 APRIL 2012 | DOI: 10.1038/NPHOTON.2012.69

Observing the localization of light in space and time by ultrafast second-harmonic microscopy

Manfred Mascheck[1], Slawa Schmidt[1], Martin Silies[1], Takashi Yatsui[2], Kokoro Kitamura[2], Motoichi Ohtsu[2], David Leipold[3], Erich Runge[3] and Christoph Lienau[1]*

Multiple coherent scattering and the constructive interference of certain scattering paths form the common scheme of several remarkable localization phenomena of classical and quantum waves in randomly disordered media[1]. Prominent examples are electron transport in disordered conductors[2,3], the localization of excitons in semiconductor nanostructures[4,5], surface plasmon polaritons at rough metallic films[6,7] or light in disordered dielectrics[8–11] and amplifying media[1,12–14]. However, direct observation of the fundamental spatiotemporal dynamics of the localization process remains challenging[15]. This holds true, in particular, for the localization of light occurring on exceedingly short femtosecond timescales and nanometre length scales. Here, we combine second harmonic microscopy with few-cycle time resolution to probe the spatiotemporal localization of light waves in a random dielectric medium. We find lifetimes of the photon modes of several femtoseconds and a broad distribution of the local optical density of states, revealing central hallmarks of the localization of light.

Multiple coherent scattering of light is both ubiquitous and elusive at the same time. Prominent examples include the colours of opals, random lasers, and the famous Brocken spectres—halo-like glories around shadow images seen on misty mountain clouds. Quite generally[16], whenever light (or any other classical or quantum-mechanical wave) interacts with a dense collection of static, random scatterers, multiple coherent scattering and wave interference results in an increased probability of it returning to the same point or to be scattered in the back-direction[10,11]. This can lead to pronounced spatial fluctuations of the local density of states (LDOS) and to wavefunctions or optical mode profiles that are exponentially localized and of fractal shape[17,18]. The energies $\hbar\omega_n$ of modes localized in the same region are strongly correlated and depend sensitively on the dimensionality and geometric size of the system as well as its symmetry with respect to time reversal. The local electric field at position $\mathbf{r}$ inside the sample can be expressed in terms of the lifetime T_{1n} and the field profile $\mathbf{E}_n(\mathbf{r})$ of the individual eigen modes:

$$\mathbf{E}(\mathbf{r}, t) = \sum\nolimits_n \mathbf{E}_n(\mathbf{r}) \exp\left(-i\omega_n t\right) \exp\left(-t/2T_{1n}\right) \qquad (1)$$

Such field intensities show unusually broad statistical distributions. Various imaging techniques have been used successfully to map field distributions[8,19] and to probe statistical signatures of photon localization[20]. Ultrasound transmission through three-dimensional media, for example, has shown a transition from a Rayleigh to a stretched exponential distribution of speckle intensities[21]. Together with the concomitant increase in fluctuations, this characterizes the transition between weak and strong localization. This is quantitatively described by predictions[22] based on one-parameter scaling[23] with the dimensionless conductance g as the natural measure of disorder strength.

Considerably less is known about temporal aspects of light localization on an ultrafast, femtosecond timescale. In the present work, we combine high-resolution nonlinear optical microscopy with few-cycle time resolution to probe the lifetimes of localized photon modes in random dielectric nanostructures. We demonstrate our approach for a densely packed disordered array of zinc oxide nanoneedles (Fig. 1a).

Zinc oxide, a wide-gap semiconductor with a bandgap of 3.3 eV, is an essentially transparent medium throughout the visible and near-infrared. With its large refractive index of $n = 1.96$ at 800 nm, it is a strong light scatterer and a prototypical random lasing material[13,14]. Moreover, ZnO nanostructures have large second-harmonic coefficients[24], making them ideal for probing the local electric field inside a sample by means of the emitted second-harmonic radiation.

We investigated randomly distributed arrays of ~300-nm-long ZnO needles with an average separation of 100 nm grown on a base of larger rods on a sapphire substrate (Fig. 1b,c). By controlling the substrate temperature[25], the needle diameter was reduced to 30–50 nm so that the needles could act as structureless point scatterers, avoiding light localization within individual needles.

We focused linearly p-polarized ultrashort 6 fs laser pulses (centre wavelength, 800 nm, far below the ZnO bandgap) to a diffraction-limited spot with a diameter of ~1 μm on the sample[26]. Local second-harmonic spectra were recorded in a reflection geometry while raster-scanning the sample through the focus. A two-dimensional map of the total, spectrally integrated second-harmonic intensity (Fig. 2a) shows pronounced spatial fluctuations. The second-harmonic emission I_{SH} is localized in certain hot spots, randomly distributed across the sample. In some spots the intensity exceeds by a factor of more than 30 the average $\langle I_{SH}\rangle$, which is dominated by a weak background, probably from the base layer. The typical diameter of a single emission spot is only 500 nm (Fig. 2b), limited by the microscope resolution. The intensity and spectral shape of the second harmonic both fluctuate from spot to spot (Fig. 2c), another strong signature of photon localization within the ZnO array[6].

To time-resolve the localized photon field, we used a pair of phase-locked and time-delayed 6 fs pulses focused to a 1 μm spot. The resulting second-harmonic emission was spectrally resolved and monitored as a function of the detection wavelength λ and the time delay τ. The resulting interferometric frequency-resolved autocorrelation (IFRAC) trace[27] can be written as

$$I_{\mathrm{IF}}(\lambda, \tau) = \left| \int E_{NL}(t, \tau) \cdot \exp(-i2\pi ct/\lambda) \mathrm{d}t \right|^2$$

[1]Institut für Physik and Center of Interface Science, Carl von Ossietzky Universität, 26129 Oldenburg, Germany, [2]School of Engineering, University of Tokyo, 113-8656 Tokyo, Japan, [3]Institut für Physik, Technische Universität Ilmenau, 98684 Ilmenau, Germany. *e-mail: christoph.lienau@uni-oldenburg.de

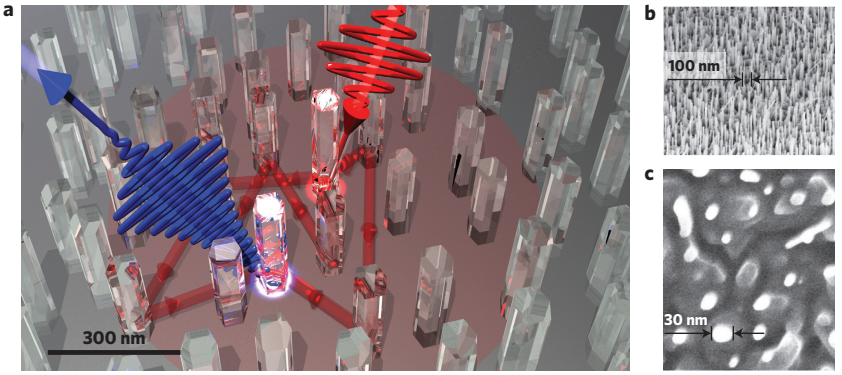

Figure 1 | Spatiotemporal localization of light in a ZnO nanoneedle array. a, An ultrashort 6 fs laser pulse centred at 800 nm is focused to its diffraction limit of ~1 μm onto an array of randomly distributed vertically aligned dielectric ZnO nanoneedles. Multiple coherent light scattering inside the array results in field localization in certain hot spots. The concomitant local field enhancement gives rise to pronounced second-harmonic emission from the ZnO needles. Experimentally, the second-harmonic emission is resolved in time, providing a measure of the lifetime of the localized light modes. **b**,**c**, Side view (**b**) and top view (**c**) scanning electron microscopy images of a needle array with an average separation of ~100 nm and a needle diameter of 30 nm.

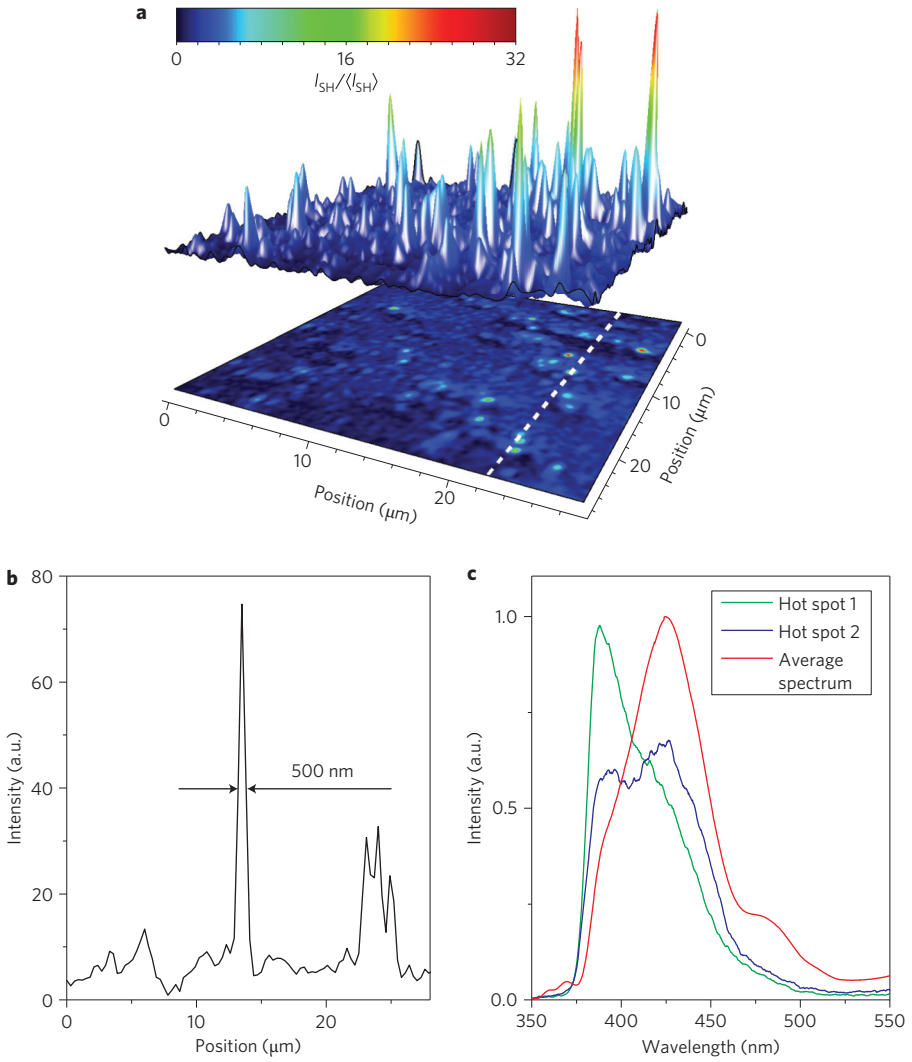

Figure 2 | Spatial intensity distribution of the second-harmonic emission. a, Confocal second-harmonic microscopy image of the nanoneedle array illuminated with 6 fs pulses at 800 nm. In the most intense local hot spots, the second-harmonic intensity is enhanced by a factor of more than 30 above the average. The overall variation of the second-harmonic intensity throughout the image reflects slight structural variations within the nanoneedle array. **b**, Cross-section along the dashed line in **a** showing that these hot spots are localized to a size of 500 nm, determined by the resolution of the microscope. **c**, Local second-harmonic emission spectra recorded inside different hot spots (green and blue solid lines) in comparison to the spatially averaged second-harmonic spectrum (red line).

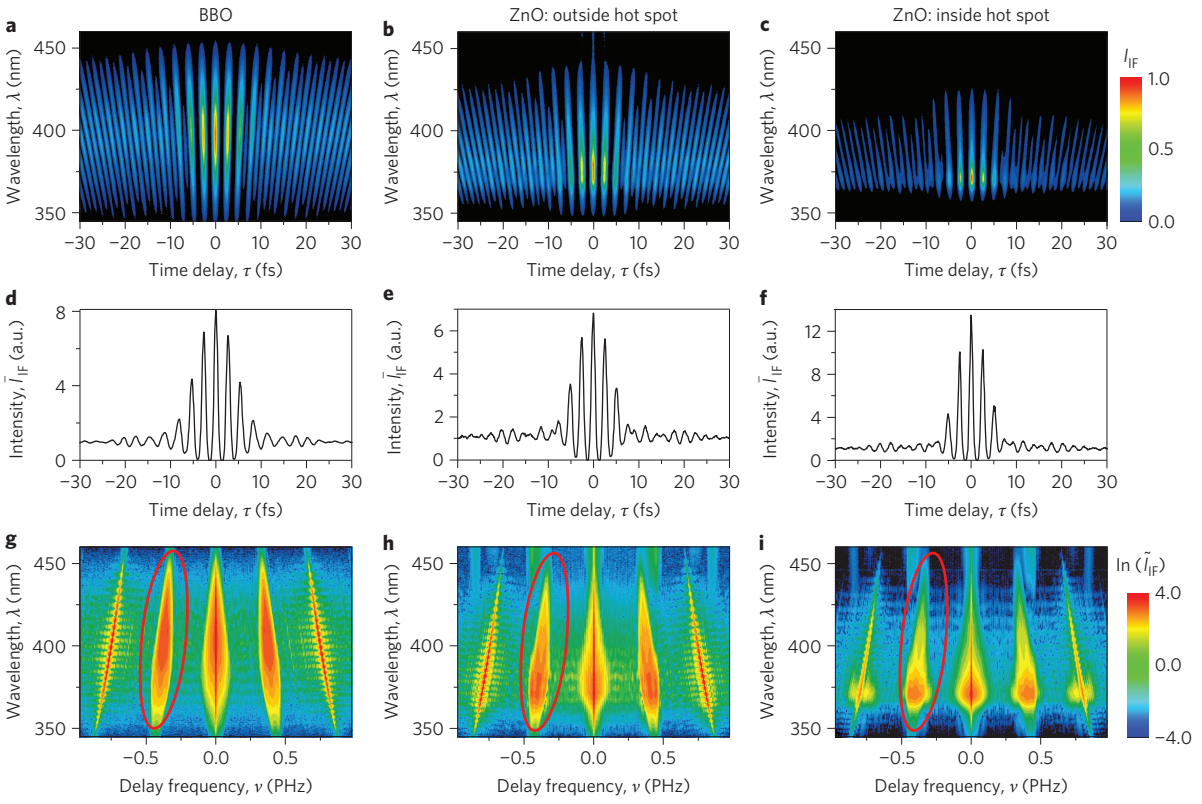

Figure 3 | IFRAC traces. a–c, The samples are illuminated with a phase-locked pair of 6 fs pulses focused to 1 μm, and IFRAC traces $I_{IF}(\lambda, \tau)$ are recorded as a function of the pulse delay τ. Data are taken from a 10-μm-thick BBO crystal used as reference (**a**) and at positions outside (**b**) and inside (**c**) a local second-harmonic hot spot on the ZnO sample. **d–f**, Corresponding spectrally integrated interferometric autocorrelation traces $\bar{I}_{IF}(\tau)$. Slight beatings at delays of ±10 and ±20 fs reflect the non-Gaussian input spectrum of the 6 fs laser pulses. **g–i**, Fourier transforms $\tilde{I}_{IF}(\lambda, \nu)$ along the time axis of the data in **a–c** plotted on a logarithmic intensity scale, showing distinct peaks at integer multiples of the first sideband $\nu = \pm c/(2\lambda)$ (marked by red ellipses). The strong reduction in spectral width of the hot spot spectrum in **c** and **i** is the signature of the increased lifetime of the localized light mode.

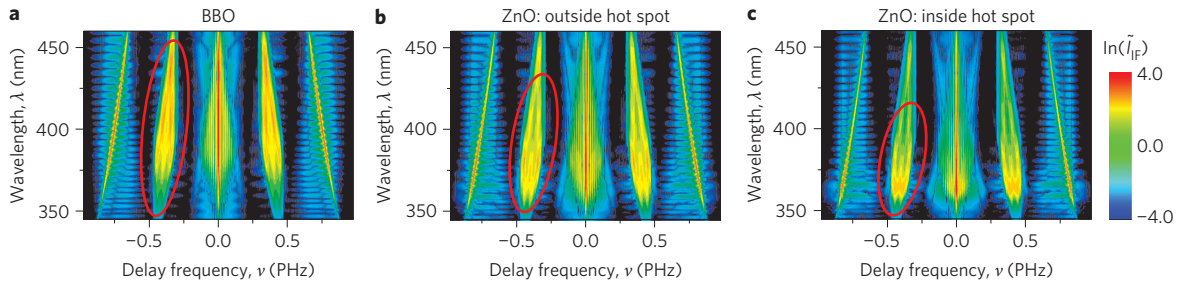

Figure 4 | Simulated Fourier transforms of IFRAC traces and reconstructed local electric fields. a–c, Fourier transforms $\tilde{I}_{IF}(\lambda, \nu)$ of IFRAC traces obtained from a Bloch equation model, describing the two-photon excitation of a two-level system by an ultrashort laser pulse. The lifetime T_1 of the two-level system is adapted to match the data in Fig. 3g–i. Lifetimes of 1.0 fs for the BBO crystal (**a**), 3.0 fs for a position outside a hot spot (**b**) and 6.5 fs for a position inside a hot spot (**c**) are deduced.

where E_{NL} is the electric field emitted from the sample illuminated by the pulse pair with field $E(t) + E(t+\tau)$. For an instantaneous second-harmonic process, $E_{NL}(t, \tau) \propto (E(t) + E(t+\tau))^2$, and the time structure of $E(t)$ can be reconstructed directly[27].

We have recorded such spectrograms from a variety of different positions inside the ZnO array. Figure 3 shows representative measurements taken from a 10-μm-thick reference beta barium borate (BBO) crystal (Fig. 3a) and positions outside (Fig. 3b) and inside (Fig. 3c) a hot spot of the ZnO array. The spectrally broad second-harmonic emission from the BBO crystal covers a range of almost 100 nm. In contrast, the spectral second-harmonic bandwidth from the ZnO array is much narrower and decreases even more when moving from a position outside to inside one of the hot spots in Fig. 2. Spectrally integrated interferometric autocorrelation traces $\bar{I}_{IF}(\tau) = \int I_{IF}(\lambda, \tau)d\lambda$ are shown in Fig. 3d–f. The marked differences between all three spectrograms are most clearly recognized by comparing Fourier transforms $\tilde{I}_{IF}(\lambda, \nu) = \int I_{IF}(\lambda, \tau)\exp(i2\pi\nu\tau)d\tau$ along the delay axis (Fig. 3g–i). In the reference measurement the spectral bandwidth of all sidebands[27] at $\nu = \pm nc/(2\lambda)$, $n = 0, 1, 2$, is substantially larger than in the nanoneedle array data. By far the smallest bandwidth is seen within one of the hotspots (Fig. 3i). This reduction in spectral width is a clear signature of the long lifetime of the localized photon modes.

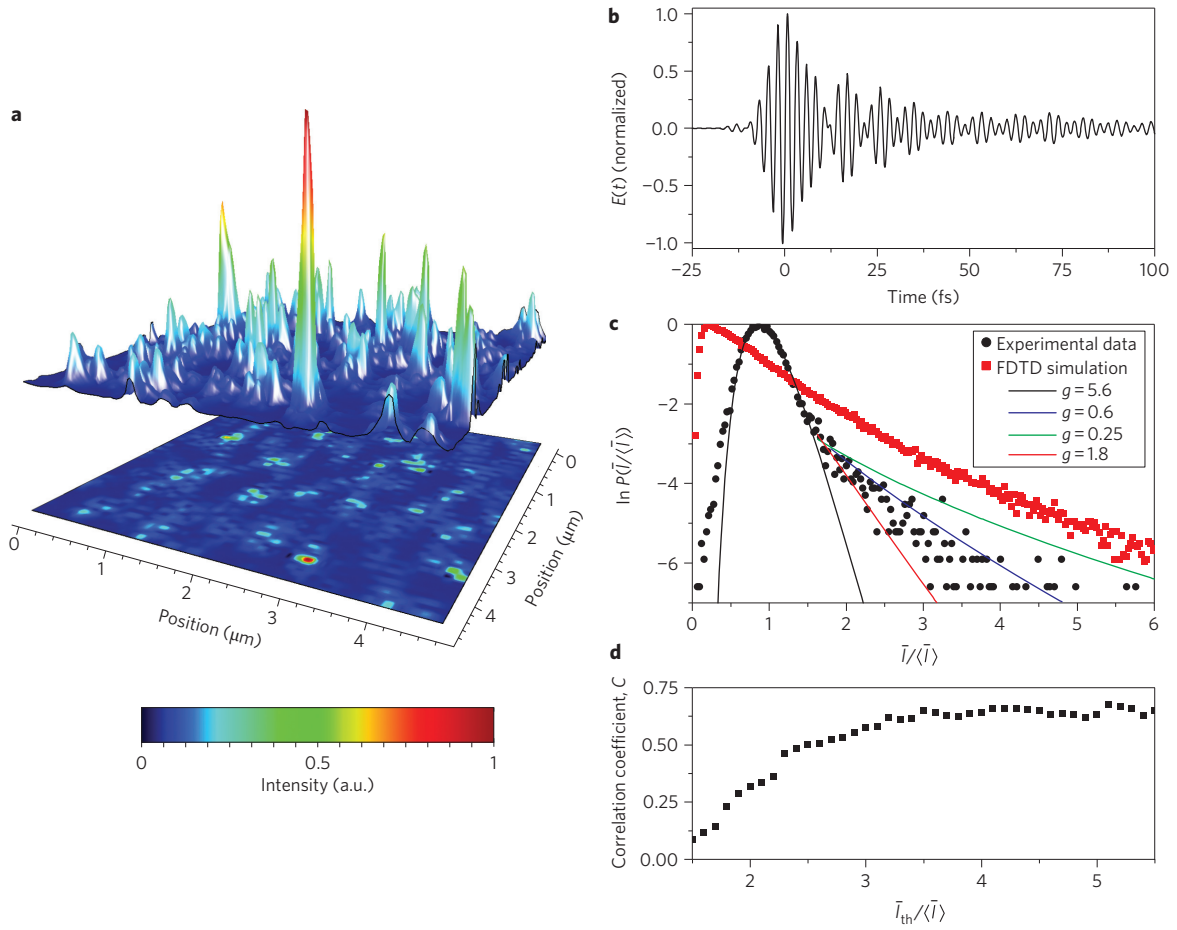

Figure 5 | Numerical solutions of Maxwell's equations for light localization inside a randomly distributed array of dielectric cylinders. a, Spatial distribution of the time-integrated second-harmonic intensity. **b**, Time structure of the electric field in one of the hot spots, suggesting a lifetime of 20 fs. **c**, Histograms of logarithms of the measured (circles) and simulated (squares) time-averaged local field intensity $\bar{I}$ at the fundamental laser wavelength. Experimental data $\bar{I}(\mathbf{r}) = I_{SH}^{1/2}(\mathbf{r})$ are taken from Fig. 2a. Both sets of data show large deviations from a Gaussian distribution at high intensities. The experimental data can be modelled by the sum of two terms given by the analytic expressions of ref. 20 with $g \approx 0.6$ (blue line) and $g \approx 5.6$ (black line). Additional curves for $g = 0.25$ and $g = 1.8$ illustrate the sensitivity. **d**, Correlation coefficient $C(I_{th})$ between photon lifetime T_1 and second-harmonic intensity I_{SH} for the experimental data in Fig. 2a, taking only those data points in **c** with intensity $\bar{I} > I_{th}$.

A weak contribution of higher-order coherent components[28] and incoherent multiphoton-induced luminescence background[24,29] to the nonlinear emission from ZnO nanostructures makes the application of direct pulse retrieval techniques[27] difficult, so we use a phenomenological Bloch equation model for data analysis[29]. We model the local nonlinear optical response of the array as that of an effective two-level system interacting with the incident laser by two-photon excitation only. The excited-state lifetime T_1, reflecting the lifetime of the local photon mode (equation (1)), is the only adjustable parameter to match the experimental data.

Simulated Fourier-transforms of IFRAC traces, shown in Fig. 4 for three different lifetimes—$T_1 = 1$ fs (Fig. 4a), 3.0 fs (Fig. 4b) and 6.5 fs (Fig. 4c)—agree quantitatively with the corresponding experimental data in Fig. 3g–i. This provides a measure of the photon mode lifetime and a reconstruction of the localized electric field $\mathbf{E}(\mathbf{r}, t)$ at the fundamental laser wavelength. Evidently, multiple coherent scattering within the disordered ZnO nanoneedle array results in a significant increase in the time duration of the local field. In some of the hot spots, the electric field, decaying at $1/(2T_1)$, persists for as long as 13 fs. Because the absorption coefficient of the ZnO film at 800 nm is less than 10 cm^{-1}, these lifetimes are not limited by absorption but rather reflect radiative out-of-plane losses.

By analysing the spectral width of the coherent second-harmonic emission spectrum, we have constructed a spatial map of the local photon mode lifetimes (Supplementary Fig. S8b), which displays random fluctuations of the T_1 time between 3 and 8 fs on a scale of 500 nm, limited by the microscope resolution. Considered in total, this map shows a negligible correlation with a simultaneously recorded map of the second-harmonic intensity (correlation coefficient $C \approx 0.1$). The correlation increases dramatically to $C \approx 0.6$ if only the points with strong second harmonic are included (Fig. 5d). This confirms the visual impression from Fig. 2a that localized states are rare events of little statistical weight at the fundamental laser frequency.

To scrutinize our results, we performed three-dimensional time-resolved simulations of Maxwell's equations for such a nanorod structure, modelled as an array of randomly distributed dielectric cylinders. A plot of the spatial distribution of the time-integrated second-harmonic intensity for a typical simulation run (Fig. 5a) displays pronounced spatial fluctuations in the second-harmonic intensity and local hot spots. The localized modes display a multifractal character[18] with field maxima predominantly located between the cylinders. They show intensity variations on a characteristic scale of 20 nm only, far beyond the experimental resolution. For sufficiently strong disorder, the average distance between adjacent hot spots reaches a few hundreds of nanometres, reflecting again the rare occurrence of strongly localized second-harmonic active modes and indicating indeed that often only an individual hot spot is probed experimentally.

The dynamics of the electric field amplitude, simulated at a distance of ~1 μm above the cylinders, is depicted in Fig. 5b. The overall decay of 20 fs matches the experiment well. At such large distances, the field dynamics display a characteristic beating pattern due to interference of a few neighbouring localized modes. This beating can be suppressed by reducing this distance, restricting the detection to fields from a single hot spot. Such beatings are not observed in Fig. 3b,c, indicating that these measurements indeed mainly probe a single localized mode. Additional arguments supporting this interpretation and ruling out alternatives, such as random lasing, are presented in Supplementary Sections S3 and S8.

Such intensity fluctuations in the LDOS are one hallmark of randomly localized modes. We therefore calculated histograms of the time-averaged local electric field intensity $\bar{I}(\mathbf{r}) = \int |E(\mathbf{r}, t)|^2 dt$ at the fundamental laser frequency from both experimental and theoretical data (Fig. 5c). Even though analytic expressions for the LDOS exist[21,30], we are not aware of predictions for the statistics of such spectrally integrated field intensities. For sufficiently strong disorder, we expect a large variance[20] and deviations from Gaussian statistics, specifically at high intensities, governed by strongly localized states. Experimentally we find a broad Gaussian around $\bar{I}/\langle\bar{I}\rangle = 1$ and a weak but pronounced approximately exponential tail at $\bar{I}/\langle\bar{I}\rangle \gg 1$. Separate measurements on the bottom layer of larger rods indicate that the second harmonic from this layer mainly leads to the Gaussian around $\bar{I}/\langle\bar{I}\rangle = 1$, confirming that second harmonic generation by modes localized within the top layer of thinner nanoneedles gives rise to the broad exponential tail in Fig. 5c. The statistics of the finite-difference time-domain (FDTD) results show a similar broad tail at $\bar{I}/\langle\bar{I}\rangle \gg 1$, decaying even slower than exponentially. The experimentally measured tail follows roughly the predictions of ref. 20 for a dimensionless conductance $g \approx 0.6$, that is, at the transition into the strong localization regime. At present, a more quantitative analysis is difficult because the exact shape of the histogram depends on the spatial resolution of the experiment and is also affected by second harmonic generation from the base of larger-diameter nanorods.

Taken together, our experimental and theoretical results present compelling evidence for light localization near the transition into the strong localization regime in an array of randomly disordered ZnO nanoneedles. We have explored the spatial and temporal aspects of this localization using a novel interferometric second-harmonic microscopic technique with few-cycle time resolution, and have directly measured lifetimes of individual localized photon modes of a few femtoseconds. This new experimental approach opens the way to the study of light localization dynamics in a variety of passive and active random media and we specifically expect it to shed new light on random lasing dynamics in ZnO nanoparticles.

Methods

ZnO sample preparation. The ZnO nanorod samples were grown by metal–organic vapour phase epitaxy (MOVPE) on a sapphire substrate[25]. By applying a two-temperature technique, ZnO rods with diameters of 30 nm and height of ~300 nm were grown on top of a base of larger rods with diameters of ~100 nm and height of ~100 nm. The density of the thinner rods was ~60 needles per μm^2, as determined by scanning electron microscopy.

IFRAC microscope. Laser pulses with a duration of 6 fs centred at a wavelength of 800 nm were derived from a Ti:sapphire oscillator (Femtolasers Rainbow) operating at a repetition rate of 82 MHz. A phase-locked pair of these pulses was generated in a dispersion-balanced Mach–Zehnder interferometer with an accuracy of <30 as using a hardware-linearized piezo scanner (Physik Instrumente P-621.1CD PIHera). Pulses with an energy of ~20 pJ were focused to their diffraction limit of 1.0 μm using an all-reflective Cassegrain objective with a numerical aperture of 0.5, fully preserving their temporal resolution[26]. The sample was placed at an oblique angle of 30° with respect to the linearly *p*-polarized incident beam, maximizing the electric field component along the ZnO needle axis and enhancing the second-harmonic signal[29]. The sample position within the focus was controlled using a three-dimensional piezo scanner (Physik Instrumente NanoCube) with a lateral resolution of 10 nm. The second-harmonic and photoluminescence emission from the sample were collected in reflection geometry, spectrally dispersed in a 0.5 m monochromator (Acton SpectraPro-2500i) and detected as a function of time delay and lateral position on the sample using a liquid-nitrogen-cooled charge coupled device (Princeton Instruments Spec-10)[29].

Optical Bloch equations modelling. We simulated the time structure of the local second-harmonic emission by solving optical Bloch equations for a two-level system interacting with the laser electric field $E(t)$ by two-photon excitation with a generalized Rabi frequency $\Omega(t) = \alpha E(t)^2/\hbar$. The excited-state lifetime T_1 gives the lifetime of the localized photon mode. Details are described in Supplementary Section S5.

FDTD simulation. Maxwell's equations for a model system were solved using a three-dimensional FDTD method using the freely available Maxwell solver Meep. Randomly distributed, vertically aligned cylindrical rods with a refractive index of $n = 1.96$, diameter of 100 nm and a randomly varied length between 0.9 and 1.0 μm were placed on top of a dielectric substrate with the refractive index of sapphire ($n = 0.175$). The needle density was chosen to be 60 needles per μm^2 to match the experimental parameters. The local second-harmonic intensity $I_{SH}(\mathbf{r}, t) = |E(\mathbf{r}, t)^2|^2$.

To simulate the incident electromagnetic field, a plane wave source at an incidence angle of 30° and with a Gaussian temporal envelope of 6 fs (full-width at half-maximum) centred at the laser wavelength of 800 nm was used. The time dynamics of the local electric field $E(\mathbf{r}, t)$ at position $\mathbf{r}$ inside a sample of area 4.3 × 4.3 μm^2 containing ~1,000 cylinders were calculated with a spatial resolution of 10 nm. Perpendicular to the cylinder axis, Bloch periodic boundary conditions were applied. At the boundaries along this axis, strongly absorbing perfectly matched layer areas were used to model open boundary conditions.

Received 24 December 2011; accepted 29 February 2012; published online 15 April 2012

References

1. Abrahams, E. (ed.) *50 Years of Anderson Localization* (World Scientific, 2010).
2. Belitz, D. & Kirkpatrick, T. R. The Anderson–Mott transition. *Rev. Mod. Phys.* **66,** 261–380 (1994).
3. Richardella, A. *et al.* Visualizing critical correlations near the metal–insulator transition in $Ga_{1-x}Mn_xAs$. *Science* **327,** 665–669 (2010).
4. Hess, H. F., Betzig, E., Harris, T. D., Pfeiffer, L. N. & West, K. W. Near-field spectroscopy of the quantum constituents of a luminescent system. *Science* **264,** 1740–1745 (1994).
5. Intonti, F. *et al.* Quantum mechanical repulsion of exciton levels in a disordered quantum well. *Phys. Rev. Lett.* **87,** 076801 (2001).
6. Gresillon, S. *et al.* Experimental observation of localized optical excitations in random metal–dielectric films. *Phys. Rev. Lett.* **82,** 4520–4523 (1999).
7. Stockman, M. I. Femtosecond optical responses of disordered clusters, composites, and rough surfaces: 'the ninth wave' effect. *Phys. Rev. Lett.* **84,** 1011–1014 (2000).
8. Sapienza, L. *et al.* Cavity quantum electrodynamics with Anderson-localized modes. *Science* **327,** 1352–1355 (2010).
9. Schwartz, T., Bartal, G., Fishman, S. & Segev, M. Transport and Anderson localization in disordered two-dimensional photonic lattices. *Nature* **446,** 52–55 (2007).
10. Albada, M. P. V. & Lagendijk, A. Observation of weak localization of light in a random medium. *Phys. Rev. Lett.* **55,** 2692–2695 (1985).
11. Wolf, P.-E. & Maret, G. Weak localization and coherent backscattering of photons in disordered media. *Phys. Rev. Lett.* **55,** 2696–2699 (1985).
12. Wiersma, D. S., van Albada, M. P. & Lagendijk, A. Coherent backscattering of light from amplifying random media. *Phys. Rev. Lett.* **75,** 1739–1742 (1995).
13. Cao, H. *et al.* Random laser action in semiconductor powder. *Phys. Rev. Lett.* **82,** 2278–2281 (1999).
14. Fallert, J. *et al.* Co-existence of strongly and weakly localized random laser modes. *Nature Photon.* **3,** 279–282 (2009).
15. Wang, J. & Genack, A. Z. Transport through modes in random media. *Nature* **471,** 345–348 (2011).
16. Sheng, P. *Introduction to Wave Scattering, Localization and Mesoscopic Phenomena* (Springer, 2006).
17. Evers, F. & Mirlin, A. D. Anderson transitions. *Rev. Mod. Phys.* **80,** 1355–1417 (2008).
18. Schreiber, M. & Grussbach, H. Multifractal wave functions at the Anderson transition. *Phys. Rev. Lett.* **67,** 607–610 (1991).
19. Riboli, F. *et al.* Anderson localization of near-visible light in two dimensions. *Opt. Lett.* **36,** 127–129 (2011).
20. Chabanov, A. A., Stoytchev, M. & Genack, A. Z. Statistical signatures of photon localization. *Nature* **404,** 850–853 (2000).
21. Hu, H., Strybulevych, A., Page, J. H., Skipetrov, S. E. & van Tiggelen, B. A. Localization of ultrasound in a three-dimensional elastic network. *Nature Phys.* **4,** 945–948 (2008).
22. Nieuwenhuizen, T. M. & van Rossum, M. C. W. Intensity distributions of waves transmitted through a multiple scattering medium. *Phys. Rev. Lett.* **74,** 2674–2677 (1995).

23. Abrahams, E., Anderson, P. W., Licciardello, D. C. & Ramakrishnan, T. V. Scaling theory of localization: absence of quantum diffusion in two dimensions. *Phys. Rev. Lett.* **42,** 673–676 (1979).
24. Djurišić, A. B. & Leung, Y. H. Optical properties of ZnO nanostructures. *Small* **2,** 944–961 (2006).
25. Kitamura, K. *et al*. Fabrication of vertically aligned ultrafine ZnO nanorods using metal–organic vapor phase epitaxy with a two-temperature growth method. *Nanotechnology* **19,** 175305 (2008).
26. Piglosiewicz, B. *et al*. Ultrasmall bullets of light-focusing few-cycle light pulses to the diffraction limit. *Opt. Express* **19,** 14451–14463 (2011).
27. Stibenz, G. & Steinmeyer, G. Interferometric frequency-resolved optical gating. *Opt. Express* **13,** 2617–2626 (2005).
28. Tritschler, T., Mücke, O. D., Wegener, M., Morgner, U. & Kärtner, F. X. Evidence for third-harmonic generation in disguise of second-harmonic generation in extreme nonlinear optics. *Phys. Rev. Lett.* **90,** 217404 (2003).
29. Schmidt, S. *et al*. Distinguishing between ultrafast optical harmonic generation and multi-photon-induced luminescence from ZnO thin films by frequency-resolved interferometric autocorrelation microscopy. *Opt. Express* **18,** 25016–25028 (2010).
30. Mirlin, A. D. Statistics of energy levels and eigenfunctions in disordered systems. *Phys. Rep.* **326,** 259–382 (2000).

Acknowledgements

This research was supported by the Japan Science and Technology Agency (JST) and the Deutsche Forschungsgemeinschaft (DFG) within the 'Nanoelectronics' programme. The authors acknowledge support in Germany by the DFG (priority programme 'Ultrafast nanooptics', SPP 1391) and by the Korea Foundation for International Cooperation of Science & Technology (Global Research Laboratory project K20815000003). Support in Japan through a Grant-in-Aid for Young Scientists (A) from MEXT and a research grant (Basic Research) from The TEPCO Memorial Foundation is also acknowledged.

Author contributions

C.L., E.R. and M.O. conceived the experiment. M.M. and S.S. carried out the measurements and analysed the data, together with M.S. and C.L. The samples were fabricated by K.K. and T.Y. FDTD simulations were performed by D.L. The manuscript was prepared by M.M., M.S., D.L., E.R. and C.L. All authors contributed to finalizing the manuscript.

Additional information

The authors declare no competing financial interests. Supplementary information accompanies this paper at www.nature.com/naturephotonics. Reprints and permission information is available online at http://www.nature.com/reprints. Correspondence and requests for materials should be addressed to C.L.